

Modeling Drinking Water UV Disinfection Reactors using PHOENICS: Comparison between Eulerian and Lagrangian Approach

Joel Ducoste, Dong Liu
North Carolina State University
208 Mann Hall CB 7098
Raleigh, NC 27695-7908

Karl Linden
Duke University
Box 90287
Durham, NC 27708-0287

Introduction

Over the years, numerical models have been developed to evaluate the disinfection effectiveness of UV systems. Perhaps the most promising numerical technique for UV system analysis is Computational Fluid Dynamics (CFD). Several researchers have used CFD for analyzing and improving the hydraulics through UV systems. Some researchers have combined particle-tracking models with CFD to predict the dose distribution (Baas, 1996; Downey et al., 1998; Buffle et al., 2000). These CFD numerical particle-tracking models are considered Lagrangian type models where the dose is determined from the time-history of each particle released in the reactor influent.

The dose as seen by each particle is calculated by integrating the fluence rate values over the particle track time history using the following equation:

$$Dose(P) = \int_0^T I(t)dt \cong \sum I \Delta t \quad (1)$$

where

Dose(P) = UV dose for particle P (J/m² or mJ/cm²)

I(t) = fluence rate (W/m² or mW/cm²)

The dose distribution is then computed by organizing the dose from all the particle track information into discrete bin sizes of different dose values. The frequency function (typically denoted as E(D)) represents the fraction of the total number of particles released in the reactor influent. Using the particle tracking method, the overall microbial inactivation can then be computed as:

$$\frac{N}{N_{o\ effluent}} = \int_0^{\infty} \frac{N}{N_o} (D)_{batch} E(D) dD \quad (2)$$

where $\frac{N}{N_o} (D)_{batch}$ represents the bench-scale microbial inactivation function determined for a specific organism. Examples of possible microbial inactivation functions are shown in

Table 1. The selection of the most appropriate inactivation function would be based on a least square fit between the experimental microbial inactivation data and the inactivation function.

Table 1: Examples of microbial inactivation models

UV Disinfection Log Survival Equations	
Chick-Watson	$\text{Ln}(N/N_o) = -kIt$
Rational	$\text{Ln}(N/N_o) = -\frac{\text{Ln}\left[1 + N_o^{x-1}(x-1)kIt\right]}{x-1}$
Selleck	$\text{Ln}(N/N_o) = -n\text{Ln}\left[1 + \frac{It}{k}\right]$
Series Event	$\text{Ln}(N/N_o) = -kIt + \text{Ln}\left[\sum_{\kappa=0}^{l-1} \frac{(kIt)^\kappa}{\kappa!}\right]$

An alternative approach to analyzing UV reactor performance with CFD is by approximating the microbial movement through the reactor as a reacting continuous variable or tracer. Early limited work using this Eulerian approach was done by Lyn et al. (1999). In their study, Lyn et al. only developed a 2-D model of the central region of an open channel reactor (i.e. no channel walls were modeled). This was done to achieve a small grid size and improve numerical accuracy. Lyn et al. used the two-equation k-ε model (Wilcox, 1998) to approximate the turbulence in the channel and assumed that microbial transport is governed by both convection and turbulent diffusion. In addition, a series-event kinetics model was used to describe microbial inactivation, which was determined from bench-scale kinetics tests from a previous study (Chiu et al., 1999a).

Lyn et al. (1999) results consistently over-predicted the effluent microbial inactivation with the over prediction less pronounced at the higher flow rates. As suggested by the authors, the most likely cause for this greater inactivation level was probably due to modeling only the central region of the channel. Chiu et al. (1999a) showed that the wall region was the main source of low inactivation due to the low fluence rate levels in that region. Another source of error pointed out by Lyn et al. may come from the turbulence model selection. The k-ε model was unable to capture the turbulence characteristics in the wake region of the lamp. One other possible source of error not mentioned by the authors may be caused by the inclusion of turbulent diffusion in the following steady-state convective-diffusion equation:

$$\rho \sum_j \frac{\partial(U_j N)}{\partial x_j} = \rho \sum_j \frac{\partial}{\partial x_j} \left(\frac{v_t}{Sc_t} \frac{\partial N}{\partial x_j} \right) + r \quad (3)$$

where N represents the number concentration of microorganisms and r represents the inactivation kinetics (Table 1). The first term on the right hand side of Equation 3 represents the transport of microorganisms by turbulent diffusion.

Diffusion can be an important component in the transport of a scalar in fluid flow as it acts to remove stark spatial differences in scalar concentration at short distances. The diffusion process causes the scalar to move from high concentrated regions to low

concentrated regions. In describing the impact of fluence rate field on the microorganism's DNA, the inactivation reaction term in the convective-diffusion equation (Equation 3) will produce low microbial concentration regions. As a result, turbulent diffusion will cause microbial movement from higher concentrated zones (i.e., zones that correspond to a low fluence rate field) to lower concentrated zones (i.e., high fluence rate zones near the UV lamps). However, since the inactivation reaction term only acts to destroy the microorganism's DNA, the concentration of microorganisms in the UV reactor should remain constant. Therefore, the inclusion of the diffusion term will cause a slight increase in the level of inactivation.

Since the Eulerian approach has not been thoroughly examined as an alternative approach to the particle tracking method, and because the Lyn et al. (1999) study was limited to modeling only the central region of the UV reactor, there is a need to still conduct an investigation of this approach for analyzing UV reactor performance. The objective of this study is to perform a comparison between the Lagrangian particle tracking approach with the Eulerian reacting tracer approach for developing the dose distribution and characterizing the UV reactor performance using CFD.

Numerical Methods

The simulation of a reacting tracer requires the solution of the conservation of mass, momentum, and convective-diffusion equations. For modeling the transport of microorganisms in a UV reactor, the diffusion term was not included. In this study, the standard two-equation k- ϵ model was used to characterize the turbulence in the UV reactor. The Eulerian reacting tracer method was used to model the open channel configuration used by Lyn et al. (1999) and the modified open channel that included baffle walls (Chiu et al., 1999b). Figure 1 displays the CFD reconstructed image for the open channel reactor. The results of the reacting tracer method will be compared to Chiu et al. (1999a, 1999b) particle tracking results.

Typically, CFD particle tracking models use a Lagrangian approach to describe the motion of particles within a flow field (Crowe et al., 1977). A detailed description of the particle flow equations and the solution technique are described by others (Crowe et al., 1977). In general, the Lagrangian equations describe the evolution of position, velocity, mass, temperature, and other scalar properties within the flow field. Particle position is simply determined from the solution to the equation $\frac{dX_p}{dt} = U_p$ where X_p is the particle position vector and U_p is the particle velocity, which is equal to a time averaged mean velocity plus a turbulent fluctuating velocity. The turbulent fluctuating velocity is calculated assuming that each velocity component follows a normal distribution with a mean of zero and a standard deviation of $\sigma = \sqrt{2k/3}$. A random number generator based on this distribution, mean, and standard deviation is used to determine the sign and magnitude of the fluctuating velocity.

In Chiu et al. (1999a, 1999b) study, a spatial homogeneous concentration of particles was released at the reactor influent. Each particle was tracked until it exits the reactor. For each time step, the UV fluence level was recorded for each particle exposed. The dose distribution curve from the particle-tracking model was combined with the Series-Event log survival equation (Table 1) through Equation 2.

The UV/CFD disinfection model used in this study is based on the turbulent convective equation plus a reaction term, which describes the disinfection inactivation

kinetics. The Series-Event disinfection inactivation kinetics term was used in the open channel flow simulation. A description of the Series event reaction kinetics is shown below:

$$r_k = kIN_{i-1} - kIN_i \quad (4)$$

In the UV/CFD disinfection model, the effluent average microbial concentration was computed as:

$$\bar{C} = \frac{\sum_{j=1}^N A_j U_j C_j}{\sum_{j=1}^N A_j U_j} \quad (5)$$

The mean concentration in Equation 5 is based on the spatial microbial concentrations in the effluent plane.

In the UV/CFD disinfection model, the effluent viable microorganism concentration was converted to an equivalent UV dose using the series-event UV disinfection log survival equation in Table 1 for the open channel reactors. The dose distribution was then computed by developing a density function based on the flow rate fraction associated with that dose. As part of this evaluation, the dose distribution based on mass rate fraction density function was also completed to determine the most appropriate method for analyzing the UV reactor performance using the Eulerian based method. The local fluence rates in the UV reactor were computed using the Line Source Integration (LSI) model (Blatchley, 1997) that includes a UV attenuation factor to account for reductions in transmittance (both in the fluid and through the quartz sleeve) and UV-c lamp efficiency (Bolton, 2000). Equation 6 displays the fluence rate relationship used in the UV/CFD model.

$$I(r, h) = \frac{P\gamma_{UV-c}\gamma_q (T_{10}')^{\alpha(r-r_q)}}{4\pi Lr} \left[A \tan\left(\frac{L/2+h}{r}\right) + A \tan\left(\frac{L/2-h}{r}\right) \right] \quad (6)$$

Modeling of Equations 4-6 was accomplished using the PLANT option of PHOENICS. A description of the Q1 file is provided at the end of this article. The following two-step strategy was used to solve the turbulent fluid flow and convective transport equations for the Eulerian UV disinfection approach:

- 1) The Reynolds average momentum equations and the k- ϵ turbulence equations with appropriate boundary conditions were solved for the given flow domain.
- 2) Assuming the solution in part 1 converges, the convective-diffusion tracer transport equations were solved given the fluid flow field determined in part 1.

This strategy of decoupling the solutions of the momentum and species transport equations improves PHOENICS ability to reach a converged solution in a shorter amount of time. It is possible to solve all the momentum and species transport equations simultaneously. However, this is not required in disinfection problems since the scalar (i.e. the reacting tracer)

does not affect the velocity field. Of course, tracer transport does depend on the velocity field solution.

The convergence of the numerical solution was based on two requirements. First, the sum of the absolute residual sources over the whole solution domain must be less than 2 percent of the reference quantities based on the total inflow for a specific variable. Second, the values of the monitored dependent variables at several locations must not change by more than 0.5 percent between successive iterations. The grid size was determined through successive refinement in the grid and evaluating the impact of that size on both the concentration profile and mean velocity profile at selected points in the UV reactor.

Results and Discussion

The UV/CFD disinfection model based on an Eulerian approach was initially computed for Chiu et al. (1999a) pilot-scale open-channel configuration without baffles. Figures 2a and 2b display the velocity vectors and local concentration of microorganisms, respectively, in a plane located at mid depth in the channel. The model was run with the same lamp power and transmittance conditions used in Chiu et al. (1999a). The influent microorganism concentration was 1 million $\#/m^3$. The approach velocity in Figure 1 was 22 cm/s. The computed mean effluent concentration was found to be 16100 $\#/m^3$, which corresponds to 1.80 log kills. These results showed good agreement with the Chiu et al.'s experimental tests, which showed 1.71 log kills.

The UV/CFD model was also computed for Chiu et al. (1999a) 25 lamp open channel setup at 8-, 12-, and 18-, and 24-cm/s approach velocities and compared with Chiu et al.'s particle tracking results. The results of this comparison are displayed in Table 2. As can be seen in Table 2, the Eulerian approach agrees well with the particle tracking method. Moreover, in Figure 2b, the Eulerian approach confirmed the observation of Chiu et al that the region near the wall was the main source of viable microorganisms in the effluent stream. In addition, the Eulerian approach also provided similar inactivation results in the central region: 5.5 log reduction in the Eulerian approach vs. 5.75 log reduction as mentioned in Chiu et al. (1999a).

Table 2: Comparison between Eulerian and particle tracking approach for log inactivation in unbaffled

Approach velocity (cm/s)	Particle tracking	Eulerian UV/CFD
8	3.4	3.7
12	2.6	2.8
18	2.0	2.0
24	1.7	1.7

Figure 3 displays the effluent dose distribution based on flow rate fraction and mass-rate fraction density function, respectively, for the unbaffled open channel with a 22 cm/s approach velocity. As discussed earlier, the Eulerian based dose distribution is calculated by converting the effluent viable microbial concentration into an equivalent dose using the appropriate log survival equation in Table 1. The results in Figure 3 show that the distribution can be significantly different depending on which density function relationship is used.

In Figure 3a, the results clearly show peaks in the low and high dose regions that were found experimentally by Chiu et al (1999a, 1999b) where their density function was computed as the fraction of the total number of particles. As in Chiu et al., the peak in the low

dose range is caused by those organisms flowing in regions near the walls while the dominant peak at the high dose region is caused by organisms flowing through the central region near the lamps. When the dose distribution is computed with a mass-rate density fraction as in Figure 3b, the peak in the high dose region does not exist because it is associated with a very small concentration of viable microorganisms in the central region of the flow. The major peak in the low dose range in Figure 3b reflects the high concentration of viable microorganism that escapes the reactor near the walls.

Figure 4 displays the velocity field and concentration of viable microorganisms in the baffled open channel reactor. In Figure 4b, the UV/CFD model predicts a lower average concentration of viable microorganisms near the wall region as a result of enhanced mixing from the presence of baffle walls. For the baffled reactor, the UV/CFD model over predicts the level of inactivation in the effluent (UV/CFD: 2.6 log kill, Chiu et al. (1999a) pilot testing: 2.2 log kill, approach velocity = 22 cm/s). One possible reason for this higher predicted log reduction may be due to the turbulence model selection.

Turbulence models, such k- ϵ model, are based on the Boussinesq effective-viscosity principle, which assumes that the turbulent stresses are equal to the product of the eddy viscosity and the mean strain rate. One of the fundamental assumptions of the eddy-viscosity turbulence based modeling is that the instantaneous turbulence production rate must equal the turbulence dissipation rate (i.e., the equilibrium hypothesis). However, if there are time-dependent structures in the flow (i.e., vortical structures behind lamps or possibly behind baffles), then the equilibrium hypothesis is violated. Other turbulence models such as the re-normalized group (RNG) k- ϵ or Reynolds stress transport model may provide a better characterization of the turbulence under non-equilibrium conditions. Therefore, the turbulence model selection may have a strong impact on the level of mixing near the baffle walls.

From the effluent concentration of viable microorganisms in the baffled reactor, the dose distribution based on the flow fraction and mass fraction were computed and displayed in Figure 5. As can be seen in Figure 5a, the flow fraction dose distribution displays a dominant peak in the high dose range. However, Chiu et al. (1999b) still found a small peak in the low dose range, which shifts slightly to higher doses. As mentioned in Chiu et al. (1999a), this subtle shift in the low dose range is due to the impact of the baffle walls on the mixing in the channel wall region. Again, the most likely reason for the Eulerian model's inability to predict the small peak even under baffle conditions is probably due to the turbulence model selection as discussed earlier.

In Figure 5b, the mass fraction dose distribution also displays only a single peak. As in Figure 4b, the mass fraction dose distribution will only accentuate the dose region corresponding to a significant concentration of viable microorganisms. More importantly, when comparing the mass distribution for both the unbaffled and baffled reactor, there is a much clearer shift in the peak of the distribution due to the presence of the baffles than when comparing the flow fraction distribution. These results suggest that the dose distribution based on the mass rate fraction may be more appropriate for evaluating UV reactor performance since it focuses on the poor-performing regions in the flow. It is this region where engineers are most interested in improving the performance of UV reactors.

While the Eulerian approach to modeling microbial inactivation and dose distribution seems comparable to the Lagrangian particle tracking approach, it is not recommended as a replacement for the particle tracking method. The Eulerian approach should be used to provide a visual display of the low dose regions in the UV reactor. In addition, the Eulerian approach could also be used to determine the mass rate fraction dose distribution, which

places a higher weighting on the dose associated with the highest concentration of viable microorganisms. As a result, engineers can investigate more effectively the impact of design changes on this low dose region.

Conclusions

A study has been done to evaluate the use of an Eulerian based approach for modeling microbial inactivation and dose distribution in UV reactors. In the Eulerian approach, microbial movement was simulated as a reacting continuous tracer with reaction kinetics based on the best-fit inactivation model for the target microorganism. The Eulerian approach was used in a baffled and an unbaffled open channel UV reactor that were used in studies by Chiu et al (1999a, 1999b). The results from the Eulerian approach simulations were compared to the microbial inactivation and dose distribution results that were produced using a Lagrangian particle tracking technique.

Overall, the effluent microbial inactivation results that were produced using the Eulerian approach agreed well with particle tracking results. Deviations between the Eulerian and particle tracking approaches might be due to the turbulence model selection. Further research using other turbulence models needs to be done to determine the impact of these models on the effluent microbial inactivation results.

The Eulerian based dose distribution was developed by converting the effluent viable microbial concentration into an equivalent dose using a disinfection log survival equation (i.e., series event model or Chick-Watson model). Two probability density functions were evaluated with the Eulerian based dose distribution: 1) density function based on cell flow rate fraction in the effluent plane and 2) density function based on the cell mass rate fraction in the effluent plane. The results showed that the flow-rate fraction density function was in good agreement with the particle tracking density function that is based on the fraction of total particles. As with the particle tracking density function, the flow-rate fraction density function produced a dominant peak in the high dose range for Chiu et al. (1999a) open channel reactor with a minor peak in the low dose range. The dominant peak in the high dose range was due to the large fraction of the flow that moves through lamp central region. For the same open channel reactor, however, the mass-rate fraction density function produced only one dominant peak in the low dose region since a larger fraction of viable microorganisms comes from the near wall regions. As a result, the mass-rate fraction density function may provide engineers with a more sensitive way of quantifying the impact of design changes on the microorganisms receiving low UV doses.

Acknowledgments

This work is funded by a grant from the American Water Works Association Research Foundation.

Nomenclature

C	Concentration of tracer	u_i	Turbulent velocity fluctuation, m/s
\bar{C}	Spatial mean concentration in a cross sectional plane	x	Spatial coordinate, m
A _j	Grid cell cross sectional area, m ²	ε	Turbulent dissipation
h	Distance from lamp center, m	ν_L	Kinematic viscosity, m ² /s
I	Fluence rate, W/m ²	γ_{UV-c}	UV-c lamp efficiency
N	Microbial concentration	γ_q	Quartz sleeve attenuation factor
P	Lamp power, W	T ₁₀	10 mm path length transmittance
L	Lamp arc length, m	r	Radial distance from lamp center

References

- Baas, M.M., 1996, Latest Advances in UV Disinfection Hydrodynamic Simulation and Relation to Practical Experiences, Proceedings AQUATECH, Amsterdam
- Blatchley III, E.R., 1997, Numerical Modeling of UV Intensity: Application to Collimated-Beam Reactors and Continuous-Flow Systems, Water Res. Vol. 31, No. 9, pg 2205
- Bolton, J.R., 2000, Calculation of Ultraviolet Fluence Rate Distribution in an Annular Reactor: Significance of Refraction and Reflection, Wat. Res. Vol. 34, No. 13, pg3315
- Buffle M.O., Chiu, K., Taghipour, F., 2000, Reactor Conceptualization and Performance Optimization with Computational Modeling, Proceedings WEF Specialty Conference on Disinfection, New Orleans, LA
- Chiu, K., Lyn, D.A., Savoye, P., Blatchley, E.R., 1999a, Integrated UV Disinfection Model Based On Particle Tracking, Journal Env. Eng. ASCE, 125(1), pg 7
- Chiu, K., Lyn, D.A., Savoye, P., Blatchley, E.R., 1999b, Effect of UV System Modifications on Disinfection Performance, Journal Env. Eng. ASCE, 125(5), pg 459
- Crowe, C.T., Sharma, M.P., Stock, D.E., 1977, The Particle-Source-In-Cell (PSI-CELL) Model for Gas-Droplet Flows, J. Fluids Engineering, 99(6), pg 325
- Downey, D., Giles, D.K., Delwiche, M.J., 1998, Finite Element Analysis of Particle and Liquid Flow Through an Ultraviolet Reactor, Computers and Electronics in Agriculture, Vol. 21, pg 81
- Lauder, B.E., Spalding, D.B., 1974, The numerical computation of turbulent flows, Computer Methods in Applied Mechanics and Engineering, 3, 269-289.
- Lyn, D.A., Chiu, K., Blatchley, E.R., 1999, Numerical Modeling of Flow and Disinfection in UV Disinfection Channels, Journal Env. Eng. ASCE, 125(1), pg 17
- Spalding, D.B., 1972, A Novel Finite-Difference Formulation for Differential Expressions Involving Both First and Second Derivatives, International Journal of Numerical Methods in Engineering, Vol 4, pg 551
- White, F. M., 1991, Viscous Fluid Flow. Second Edition, McGraw-Hill, New York
- Wilcox, D. C., 1998, Turbulence Modeling for CFD, DCW Industries, LaCanada, CA

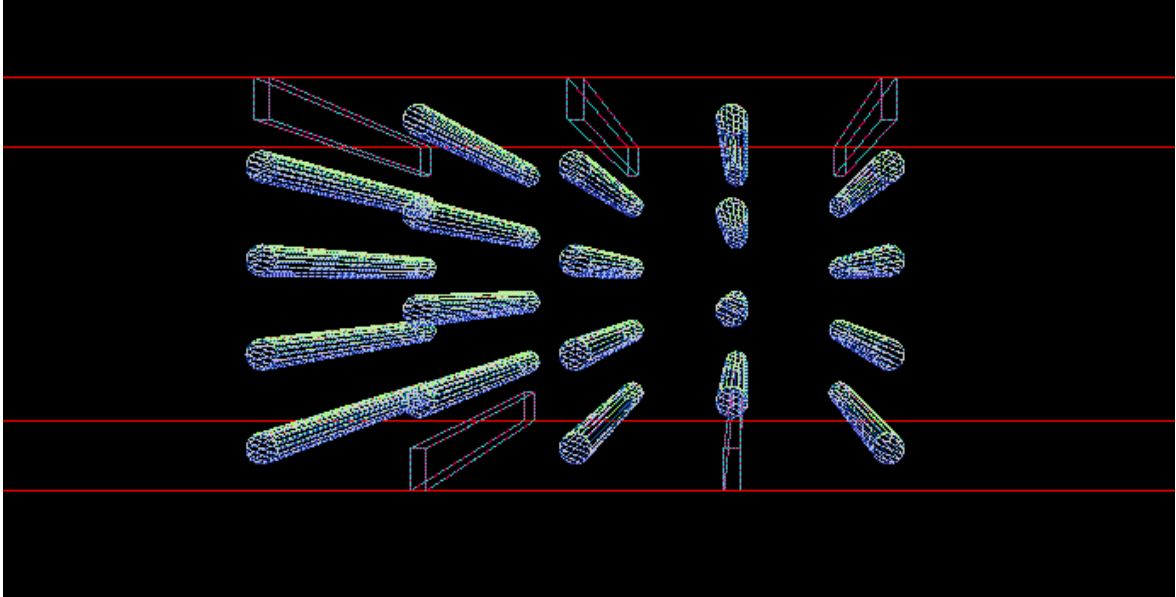
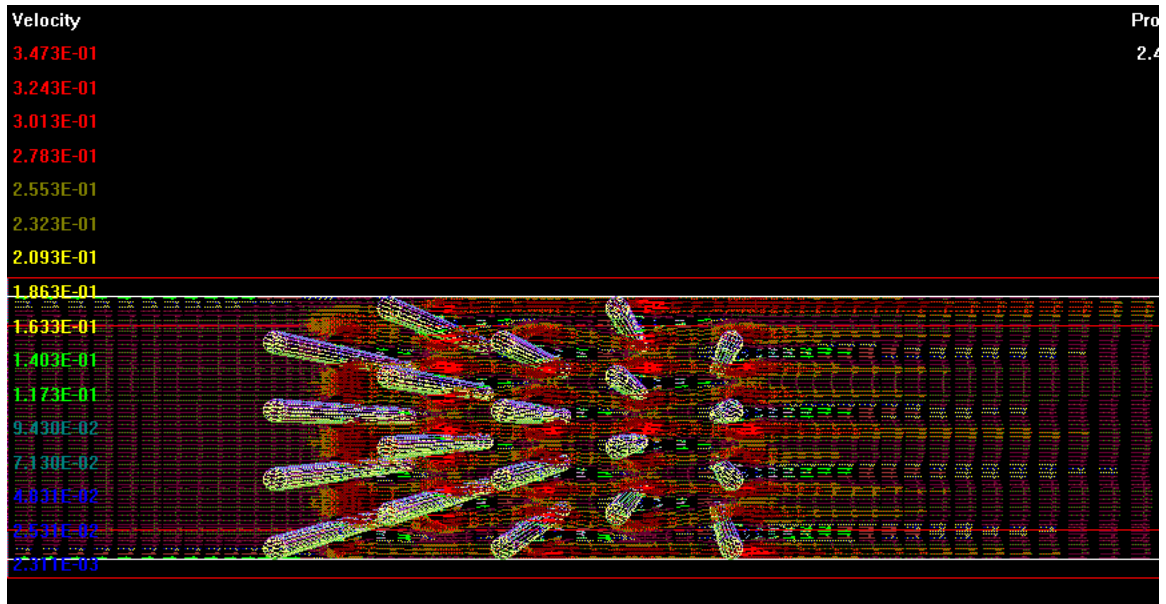


Figure 1. CFD Representation of Chiu et al. (1999a) open channel UV reactor

a



b

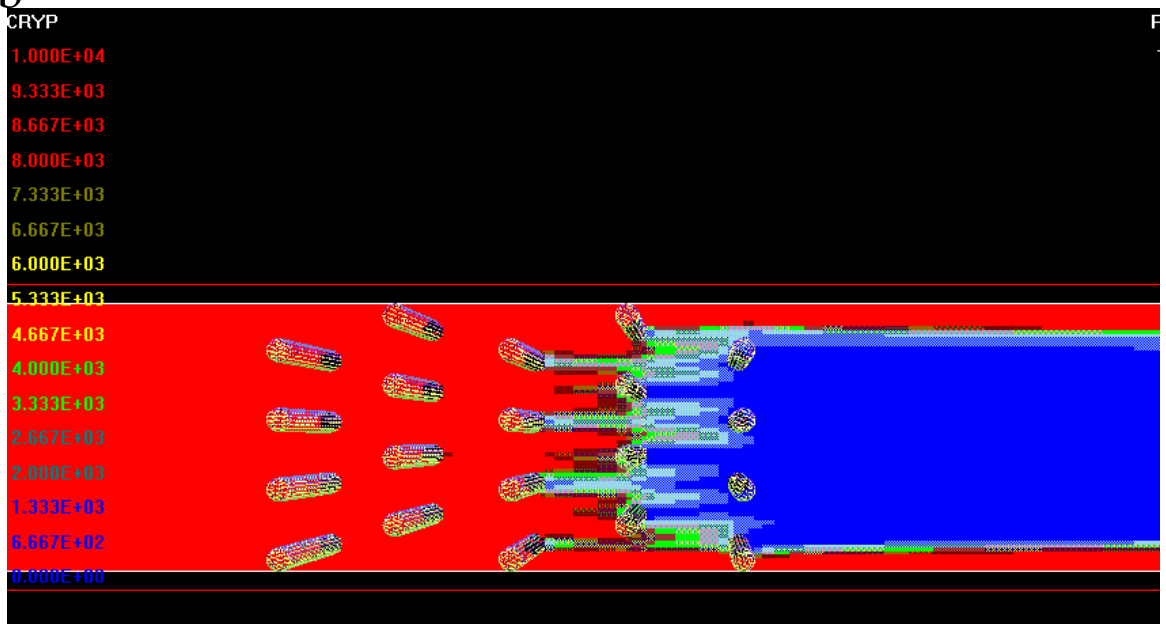


Figure 2: CFD unbauffed open channel UV Reactors: a) velocity vectors, b) viable microbial contours

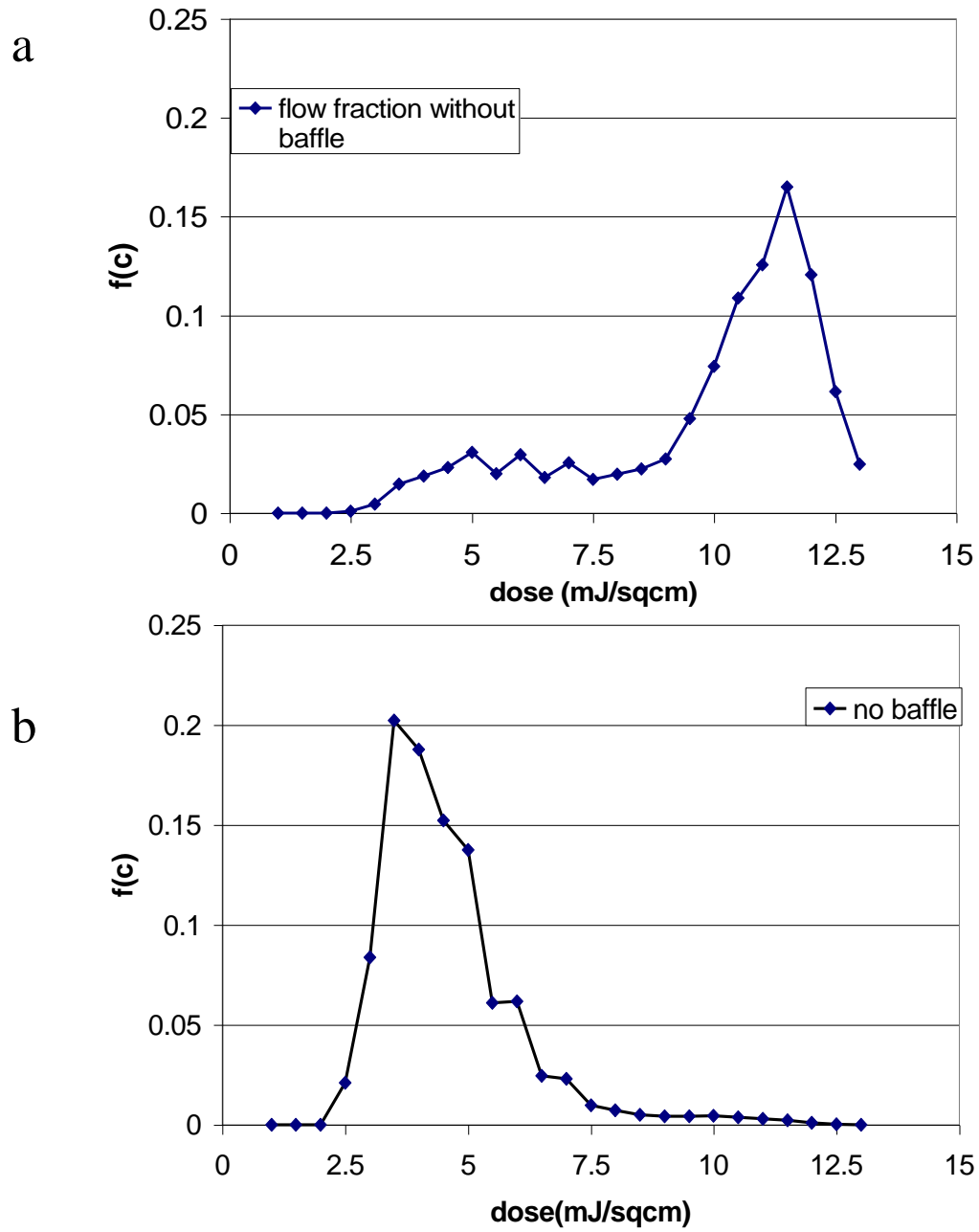


Figure 3. Comparison of dose distribution from Eulerian approach in unbaffled open channel reactor: a) Flow rate Fraction, b) Mass rate fraction

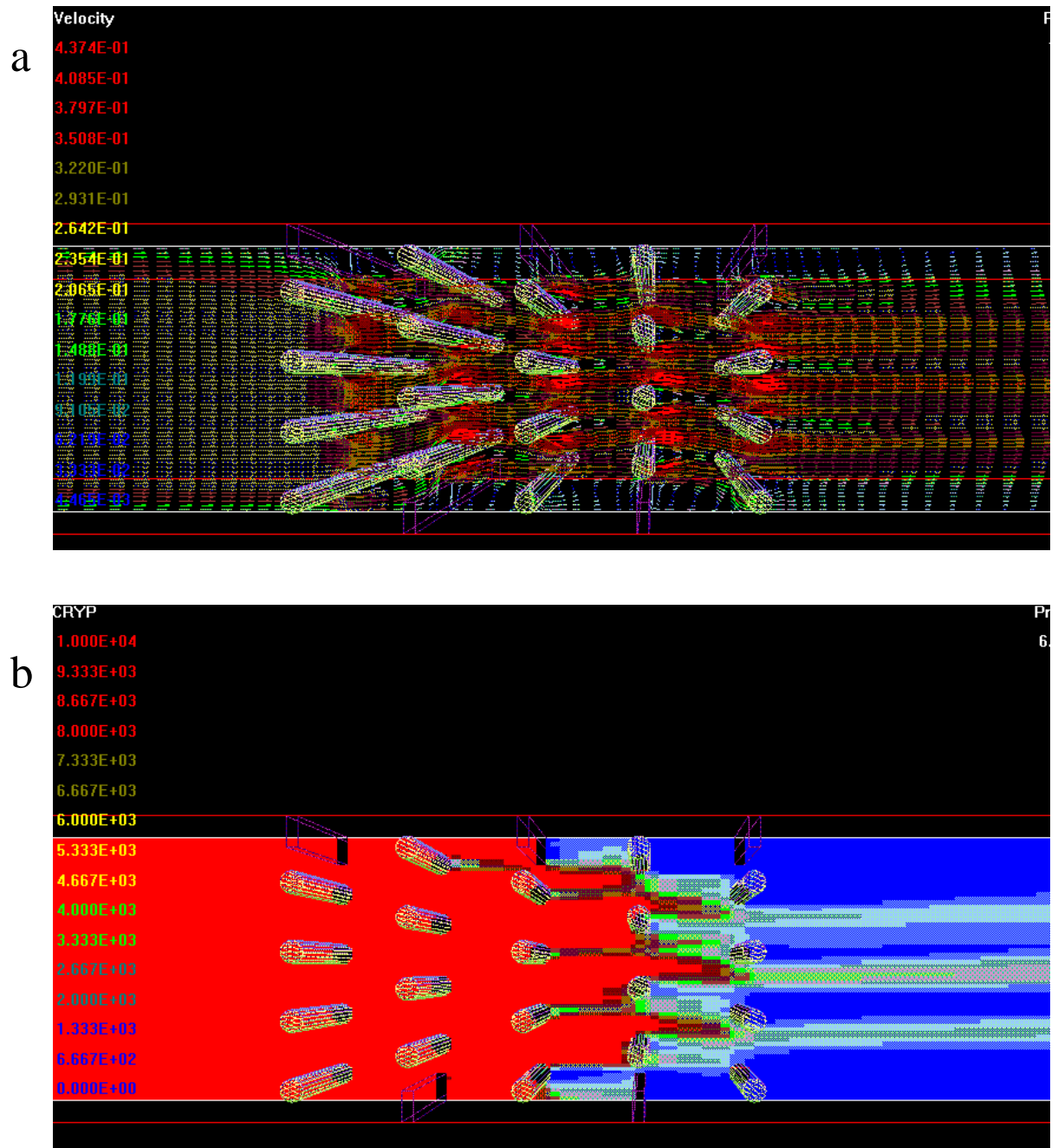


Figure 4. CFD baffled open channel UV Reactors: a) velocity vectors, b) viable microbial contours

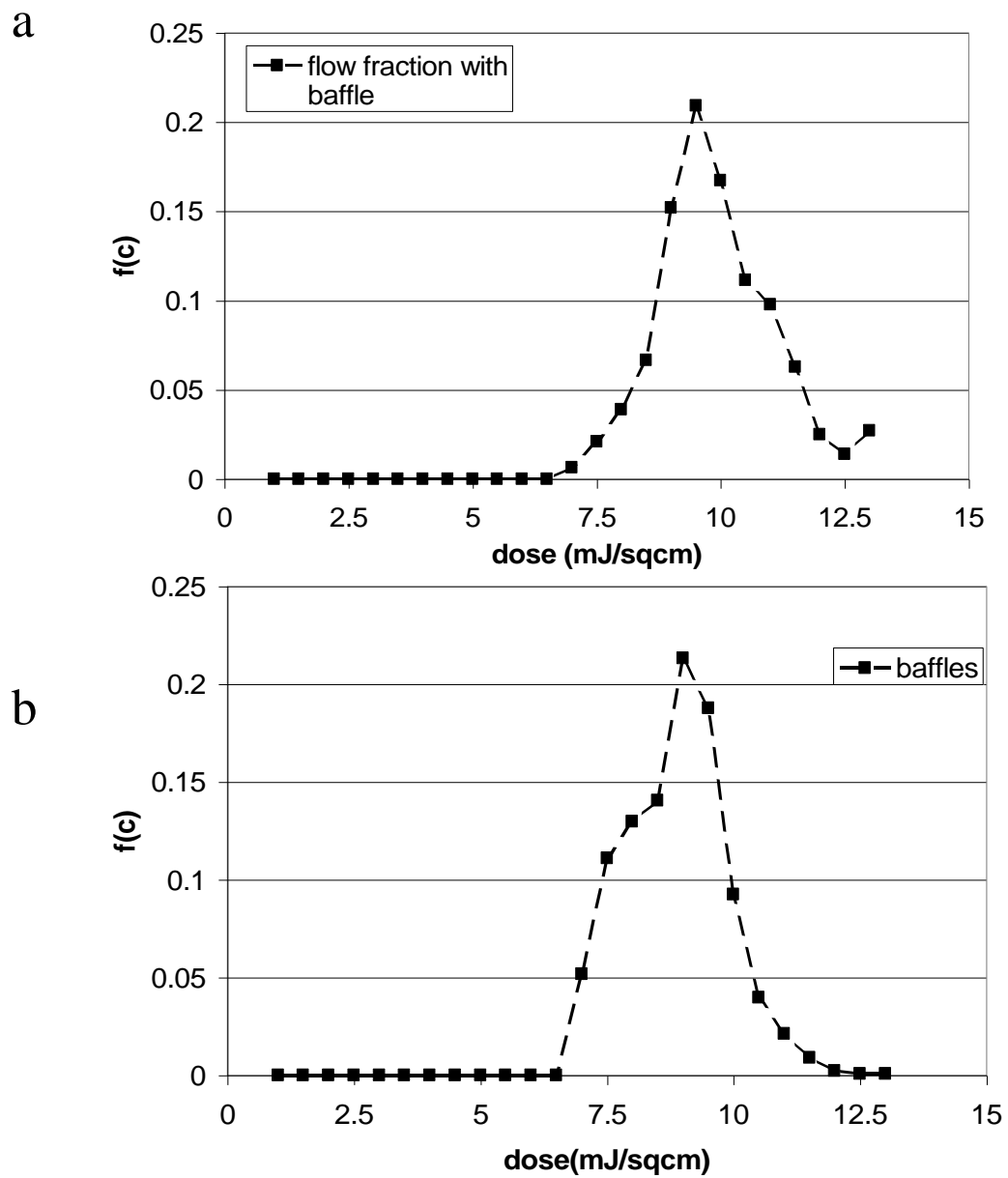


Figure 5. Comparison of dose distribution from Eulerian approach in baffled open channel reactor: a) Flow rate Fraction, b) Mass rate fraction

Sample Q1 file for Modeling UV Reactors

UV reacting tracer model Q1

Q1 created by VDI menu, Version 3.3, Date 10/02/00

CPVNAM=VDI;SPPNAM=Core

IRUNN = 1 ;LIBREF = 0

Group 1. Run Title

TEXT(20 LAMP UV BAFFLED Reactor FLUENCE AND MICROBE)

Group 2. Transience

STEADY = T

Groups 3, 4, 5 Grid Information

* Overall number of cells, RSET(M,NX,NY,NZ,tolerance)

RSET(M,133,66,15)

* Set overall domain extent:

* xulast yvlast zwlast

name

XSI= 3.800000E+00; YSI= 3.300000E-01; ZSI= 7.600000E-01

RSET(D,CHAM)

Group 6. Body-Fitted coordinates

Group 7. Variables: STOREd,SOLVEd,NAMED

ONEPHS = T

* Solved variables list

SOLVE(C1, C2, C3, C4)

SOLVE(C5,C6,C7,C8,C9,C10,C11)

* Stored variables list

STORE(EPKE,AFD1,ACD1,cryp,cmas,flu)

STORE(RR1,HH1,RR2,RR3,RR4,RR5,RR6,RR7,RR8,RR9,RR10,RR11)

STORE(RR12,RR13,RR14,RR15,RR16,RR17,RR18,RR19,RR20,RR21)

STORE(RR22,RR23,RR24,RR25)

STORE(P1, U1 ,V1 ,W1)

* Additional solver options

TURMOD(KEMODL)

STORE(KE,EP)

Group 8. Terms & Devices

TERMS (C1 ,Y,N,N,N,Y,N)

TERMS (C2 ,Y,Y,N,N,Y,N)

TERMS (C3 ,Y,Y,N,N,Y,N)

TERMS (C4 ,Y,Y,N,N,Y,N)

TERMS (C5 ,Y,N,N,N,Y,N)

TERMS (C6 ,Y,N,N,N,Y,N)

TERMS (C7 ,Y,N,N,N,Y,N)

TERMS (C8 ,Y,N,N,N,Y,N)

TERMS (C9 ,Y,N,N,N,Y,N)

TERMS (C10 ,Y,N,N,N,Y,N)

TERMS (C11 ,Y,N,N,N,Y,N)

Group 9. Properties

RHO1 = 9.982300E+02

CP1 = 4.181800E+03

ENUL = 1.006000E-06

Group 10. Inter-Phase Transfer Processes

Group 11. Initialise Var/Porosity Fields

No PATCHes used for this Group

INIADD = F

Group 12. Convection and diffusion adjustments

No PATCHes used for this Group

Group 13. Boundary & Special Sources

** DEFINE LOCATION OF UV LAMPS

XL1=2.0;YL1=0.03375

XL2=2.0;YL2=0.10875

XL3=2.0;YL3=0.18375

XL4=2.0;YL4=0.25875

XL6=2.125;YL6=0.1435

XL7=2.125;YL7=0.071

XL8=2.125;YL8=0.221

XL9=2.125;YL9=0.296

XL11=2.25;YL11=0.03375

XL12=2.25;YL12=0.10875

XL13=2.25;YL13=0.18375

XL14=2.25;YL14=0.25875

XL16=2.375;YL16=0.1435

XL17=2.375;YL17=0.071

XL18=2.375;YL18=0.221

XL19=2.375;YL19=0.296

XL21=2.5;YL21=0.03375

XL22=2.5;YL22=0.10875

XL23=2.5;YL23=0.18375

XL24=2.5;YL24=0.25875

RG(1)=XL1;RG(2)=YL1

RG(3)=XL2;RG(4)=YL2

RG(5)=XL3;RG(6)=YL3

RG(7)=XL4;RG(8)=YL4

RG(11)=XL6;RG(12)=YL6

RG(13)=XL7;RG(14)=YL7

RG(15)=XL8;RG(16)=YL8

RG(17)=XL9;RG(18)=YL9

RG(21)=XL11;RG(22)=YL11

RG(23)=XL12;RG(24)=YL12

RG(25)=XL13;RG(26)=YL13

RG(27)=XL14;RG(28)=YL14

RG(31)=XL16;RG(32)=YL16

RG(33)=XL17;RG(34)=YL17

RG(35)=XL18;RG(36)=YL18

RG(37)=XL19;RG(38)=YL19

RG(41)=XL21;RG(42)=YL21

RG(43)=XL22;RG(44)=YL22

RG(45)=XL23;RG(46)=YL23

RG(47)=XL24;RG(48)=YL24

ZL1=0.38;RG(51)=ZL1

LL=0.760;LR=0.0125

RG(52)=LL;RG(53)=LR

LPW1=26.7;TRNB=0.65

RG(54)=LPW1;RG(55)=TRNB

TRNI=0.502;RG(59)=TRNI
QRTZ=0.0015;RG(75)=QRTZ
PI=3.14159265
RG(56)=PI
APOW=100.00;RG(70)=APOW
UVEF=0.40;RG(57)=UVEF
COEF=1.00
KK=0.1107;RG(58)=COEF*KK

PLANTBEGIN

<SC0601> RR1=((XG2D-RG(1))**2.+(YG2D-RG(2))**2.)**0.5
<SC0602> RR2=((XG2D-RG(3))**2.+(YG2D-RG(4))**2.)**0.5
<SC0603> RR3=((XG2D-RG(5))**2.+(YG2D-RG(6))**2.)**0.5
<SC0604> RR4=((XG2D-RG(7))**2.+(YG2D-RG(8))**2.)**0.5
<SC0606> RR6=((XG2D-RG(11))**2.+(YG2D-RG(12))**2.)**0.5
<SC0607> RR7=((XG2D-RG(13))**2.+(YG2D-RG(14))**2.)**0.5
<SC0608> RR8=((XG2D-RG(15))**2.+(YG2D-RG(16))**2.)**0.5
<SC0609> RR9=((XG2D-RG(17))**2.+(YG2D-RG(18))**2.)**0.5
<SC0611> RR11=((XG2D-RG(21))**2.+(YG2D-RG(22))**2.)**0.5
<SC0612> RR12=((XG2D-RG(23))**2.+(YG2D-RG(24))**2.)**0.5
<SC0613> RR13=((XG2D-RG(25))**2.+(YG2D-RG(26))**2.)**0.5
<SC0614> RR14=((XG2D-RG(27))**2.+(YG2D-RG(28))**2.)**0.5
<SC0616> RR16=((XG2D-RG(31))**2.+(YG2D-RG(32))**2.)**0.5
<SC0617> RR17=((XG2D-RG(33))**2.+(YG2D-RG(34))**2.)**0.5
<SC0618> RR18=((XG2D-RG(35))**2.+(YG2D-RG(36))**2.)**0.5
<SC0619> RR19=((XG2D-RG(37))**2.+(YG2D-RG(38))**2.)**0.5
<SC0621> RR21=((XG2D-RG(41))**2.+(YG2D-RG(42))**2.)**0.5
<SC0622> RR22=((XG2D-RG(43))**2.+(YG2D-RG(44))**2.)**0.5
<SC0623> RR23=((XG2D-RG(45))**2.+(YG2D-RG(46))**2.)**0.5
<SC0624> RR24=((XG2D-RG(47))**2.+(YG2D-RG(48))**2.)**0.5
<SC0626> HH1=ABS(ZGNZ-RG(51)+TINY)
<SC0627> FLU=C1+C5+C6+C7+C8+C9+C10+C11

PATCH(IRR1,CELL,1,NX,1,NY,1,NZ,1,LSTEP)

<SORC58> VAL=RG(54)*(RG(59)**(RG(70)*RG(75)))*\$
(RG(55)**(RG(70)*ABS(RR1-RG(53)))*RG(57)/\$
(4.*RG(56)*RG(52)*RR1)*\$
(ATAN((RG(52)/2.+HH1)/RR1)+ATAN((RG(52)/2.-HH1)/RR1))+\$
RG(54)*(RG(59)**(RG(70)*RG(75)))*\$
(RG(55)**(RG(70)*ABS(RR2-RG(53)))*RG(57)/\$
(4.*RG(56)*RG(52)*RR2)*\$
(ATAN((RG(52)/2.+HH1)/RR2)+ATAN((RG(52)/2.-HH1)/RR2))+\$
RG(54)*(RG(59)**(RG(70)*RG(75)))*\$
(RG(55)**(RG(70)*ABS(RR3-RG(53)))*RG(57)/\$
(4.*RG(56)*RG(52)*RR3)*\$
(ATAN((RG(52)/2.+HH1)/RR3)+ATAN((RG(52)/2.-HH1)/RR3))

COVAL(IRR1,C1,FIXVAL,GRND)

PATCH(IRR2,CELL,1,NX,1,NY,1,NZ,1,LSTEP)

<SORC86> VAL=RG(54)*(RG(59)**(RG(70)*RG(75)))*\$
(RG(55)**(RG(70)*ABS(RR4-RG(53)))*RG(57)/\$
(4.*RG(56)*RG(52)*RR4)*\$
(ATAN((RG(52)/2.+HH1)/RR4)+ATAN((RG(52)/2.-HH1)/RR4))+\$
RG(54)*(RG(59)**(RG(70)*RG(75)))*\$
(RG(55)**(RG(70)*ABS(RR6-RG(53)))*RG(57)/\$
(4.*RG(56)*RG(52)*RR6)*\$
(ATAN((RG(52)/2.+HH1)/RR6)+ATAN((RG(52)/2.-HH1)/RR6))

COVAL(IRR2,C5,FIXVAL,GRND)

PATCH(IRR3,CELL,1,NX,1,NY,1,NZ,1,LSTEP)

<SORC99> VAL=RG(54)*(RG(59)**(RG(70)*RG(75)))*\$
(RG(55)**(RG(70)*ABS(RR7-RG(53)))*RG(57)/\$

(4.*RG(56)*RG(52)*RR7)*\$
 (ATAN((RG(52)/2.+HH1)/RR7)+ATAN((RG(52)/2.-HH1)/RR7))+\$
 RG(54)*RG(59)**(RG(70)*RG(75))*\$
 (RG(55)**(RG(70)*ABS(RR8-RG(53)))*RG(57)/\$
 (4.*RG(56)*RG(52)*RR8)*\$
 (ATAN((RG(52)/2.+HH1)/RR8)+ATAN((RG(52)/2.-HH1)/RR8))+\$
 RG(54)*RG(59)**(RG(70)*RG(75))*\$
 (RG(55)**(RG(70)*ABS(RR9-RG(53)))*RG(57)/\$
 (4.*RG(56)*RG(52)*RR9)*\$
 (ATAN((RG(52)/2.+HH1)/RR9)+ATAN((RG(52)/2.-HH1)/RR9))
 COVAL(IRR3,C6,FIXVAL,GRND)
 PATCH(IRR4,CELL,1,NX,1,NY,1,NZ,1,LSTEP)
 <SORC57> VAL=RG(54)*RG(59)**(RG(70)*RG(75))*\$
 (RG(55)**(RG(70)*ABS(RR11-RG(53)))*RG(57)/\$
 (4.*RG(56)*RG(52)*RR11)*\$
 (ATAN((RG(52)/2.+HH1)/RR11)+ATAN((RG(52)/2.-HH1)/RR11))+\$
 RG(54)*RG(59)**(RG(70)*RG(75))*\$
 (RG(55)**(RG(70)*ABS(RR12-RG(53)))*RG(57)/\$
 (4.*RG(56)*RG(52)*RR12)*\$
 (ATAN((RG(52)/2.+HH1)/RR12)+ATAN((RG(52)/2.-HH1)/RR12))
 COVAL(IRR4,C7,FIXVAL,GRND)
 PATCH(IRR5,CELL,1,NX,1,NY,1,NZ,1,LSTEP)
 <SORC25> VAL=RG(54)*RG(59)**(RG(70)*RG(75))*\$
 (RG(55)**(RG(70)*ABS(RR13-RG(53)))*RG(57)/\$
 (4.*RG(56)*RG(52)*RR13)*\$
 (ATAN((RG(52)/2.+HH1)/RR13)+ATAN((RG(52)/2.-HH1)/RR13))+\$
 RG(54)*RG(59)**(RG(70)*RG(75))*\$
 (RG(55)**(RG(70)*ABS(RR14-RG(53)))*RG(57)/\$
 (4.*RG(56)*RG(52)*RR14)*\$
 (ATAN((RG(52)/2.+HH1)/RR14)+ATAN((RG(52)/2.-HH1)/RR14))
 COVAL(IRR5,C8,FIXVAL,GRND)
 PATCH(IRR6,CELL,1,NX,1,NY,1,NZ,1,LSTEP)
 <SORC31> VAL=RG(54)*RG(59)**(RG(70)*RG(75))*\$
 (RG(55)**(RG(70)*ABS(RR16-RG(53)))*RG(57)/\$
 (4.*RG(56)*RG(52)*RR16)*\$
 (ATAN((RG(52)/2.+HH1)/RR16)+ATAN((RG(52)/2.-HH1)/RR16))+\$
 RG(54)*RG(59)**(RG(70)*RG(75))*\$
 (RG(55)**(RG(70)*ABS(RR17-RG(53)))*RG(57)/\$
 (4.*RG(56)*RG(52)*RR17)*\$
 (ATAN((RG(52)/2.+HH1)/RR17)+ATAN((RG(52)/2.-HH1)/RR17))+\$
 RG(54)*RG(59)**(RG(70)*RG(75))*\$
 (RG(55)**(RG(70)*ABS(RR18-RG(53)))*RG(57)/\$
 (4.*RG(56)*RG(52)*RR18)*\$
 (ATAN((RG(52)/2.+HH1)/RR18)+ATAN((RG(52)/2.-HH1)/RR18))
 COVAL(IRR6,C9,FIXVAL,GRND)
 PATCH(IRR7,CELL,1,NX,1,NY,1,NZ,1,LSTEP)
 <SORC37> VAL=RG(54)*RG(59)**(RG(70)*RG(75))*\$
 (RG(55)**(RG(70)*ABS(RR19-RG(53)))*RG(57)/\$
 (4.*RG(56)*RG(52)*RR19)*\$
 (ATAN((RG(52)/2.+HH1)/RR19)+ATAN((RG(52)/2.-HH1)/RR19))+\$
 RG(54)*RG(59)**(RG(70)*RG(75))*\$
 (RG(55)**(RG(70)*ABS(RR21-RG(53)))*RG(57)/\$
 (4.*RG(56)*RG(52)*RR21)*\$
 (ATAN((RG(52)/2.+HH1)/RR21)+ATAN((RG(52)/2.-HH1)/RR21))
 COVAL(IRR7,C10,FIXVAL,GRND)
 PATCH(IRR8,CELL,1,NX,1,NY,1,NZ,1,LSTEP)
 <SORC43> VAL=RG(54)*RG(59)**(RG(70)*RG(75))*\$
 (RG(55)**(RG(70)*ABS(RR22-RG(53)))*RG(57)/\$

```

(4.*RG(56)*RG(52)*RR22)*$
(ATAN((RG(52)/2.+HH1)/RR22)+ATAN((RG(52)/2.-HH1)/RR22))+$
RG(54)*(RG(59))**(RG(70)*RG(75))*$
(RG(55))**(RG(70)*ABS(RR23-RG(53)))*RG(57)/$
(4.*RG(56)*RG(52)*RR23)*$
(ATAN((RG(52)/2.+HH1)/RR23)+ATAN((RG(52)/2.-HH1)/RR23))+$
RG(54)*(RG(59))**(RG(70)*RG(75))*$
(RG(55))**(RG(70)*ABS(RR24-RG(53)))*RG(57)/$
(4.*RG(56)*RG(52)*RR24)*$
(ATAN((RG(52)/2.+HH1)/RR24)+ATAN((RG(52)/2.-HH1)/RR24))
COVAL(IRR8,C11,FIXVAL,GRND)
PATCH(ORG1,PHASEM,1,NX,1,NY,1,NZ,1,LSTEP)
<SORC51> CO=FLU*RG(58)
COVAL(ORG1,C2,GRND,0.0)
PATCH(ORG2,PHASEM,1,NX,1,NY,1,NZ,1,LSTEP)
<SORC53> VAL=FLU*RG(58)*C2-FLU*RG(58)*C3
COVAL(ORG2,C3,FIXFLU,GRND)
PATCH(ORG3,PHASEM,1,NX,1,NY,1,NZ,1,LSTEP)
<SORC55> VAL=FLU*RG(58)*C3
COVAL(ORG3,C4,FIXFLU,GRND)
PLANTEND

```

```

Parent VR object for this patch is: INLET
PATCH(OB1 ,WEST , 1, 1, 1, 66, 1, 15, 1, 1)
COVAL(OB1 ,P1 , FIXFLU , 2.395752E+02)
COVAL(OB1 ,U1 , 0.000000E+00, 2.200000E-01)
COVAL(OB1 ,V1 , 0.000000E+00, 0.000000E+00)
COVAL(OB1 ,W1 , 0.000000E+00, 0.000000E+00)
COVAL(OB1 ,KE , 0.000000E+00, 1.440000E-04)
COVAL(OB1 ,EP , 0.000000E+00, 1.259520E-05)
COVAL(OB1 ,C1 , 0.000000E+00, 0.0)
COVAL(OB1 ,C2 , 0.000000E+00, 1.000000E+06)
COVAL(OB1 ,C3 , 0.000000E+00, 0.000000E+00)
COVAL(OB1 ,C4 , 0.000000E+00, 0.000000E+00)
PATCH(OB2 ,EAST , 133, 133, 1, 66, 1, 15, 1, 1)
COVAL(OB2 ,P1 , 1.000000E+03, 0.000000E+00)
COVAL(OB2 ,U1 , 0.000000E+00, 0.000000E+00)
COVAL(OB2 ,V1 , 0.000000E+00, 0.000000E+00)
COVAL(OB2 ,W1 , 0.000000E+00, 0.000000E+00)
COVAL(OB2 ,KE , 0.000000E+00, SAME )
COVAL(OB2 ,EP , 0.000000E+00, SAME )
COVAL(OB2 ,C1 , 0.000000E+00, 0.0)
COVAL(OB2 ,C2 , 0.000000E+00, 0.000000E+00)
COVAL(OB2 ,C3 , 0.000000E+00, 0.000000E+00)
COVAL(OB2 ,C4 , 0.000000E+00, 0.000000E+00)

```

Group 14. Downstream Pressure For PARAB

Group 15. Terminate Sweeps

LSWEEP = 600

Group 16. Terminate Iterations

Group 17. Relaxation

```

RELAX(C1 ,FALSDT, 1000.)
RELAX(C2 ,LINRLX, 0.05)
RELAX(C3 ,LINRLX, 0.05)
RELAX(C4 ,LINRLX, 0.05)
RELAX(C5 ,FALSDT, 1000.)

```

```

RELAX(C6 ,FALSDT, 1000.)
RELAX(C7 ,FALSDT, 1000.)
RELAX(C8 ,FALSDT, 1000.)
RELAX(C9 ,FALSDT, 1000.)
RELAX(C10 ,FALSDT, 1000.)
RELAX(C11 ,FALSDT, 1000.)
KELIN = 3
*****

Group 18. Limits
*****

Group 19. EARTH Calls To GROUND Station
USEGRD = T ;USEGRX = T
GENK = T
NAMSAT =MOSG
*****

Group 20. Preliminary Printout
ECHO = T
*****

Group 21. Print-out of Variables
*****

Group 22. Monitor Print-Out
*****

Group 23.Field Print-Out & Plot Control
NPRINT = 100000
ISWPRF = 1 ;ISWPRL = 100000
*****

Group 24. Dumps For Restarts
NOWIPE = T

GVIEW(P,0.000000E+00,0.000000E+00,1.000000E+00)
GVIEW(UP,0.000000E+00,1.000000E+00,0.000000E+00)

> DOM, SIZE, 3.800000E+00, 3.300000E-01, 7.600000E-01
> DOM, MONIT, 2.509380E+00, 2.618750E-01, 5.320000E-01
> DOM, SCALE, 1.000000E+00, 1.000000E+00, 1.000000E+00
> DOM, SNAPSIZ, 1.000000E-02
> GRID, RSET_X_1, -63, 1.500000E+00
> GRID, RSET_X_5, -5, 1.650000E+00
> GRID, RSET_X_9, -5, 1.650000E+00
> GRID, RSET_X_13, -5, 1.650000E+00
> GRID, RSET_X_17, -5, 1.650000E+00
> GRID, RSET_X_21, 35, 1.500000E+00
> GRID, RSET_Z_1, 15, 1.000000E+00
> DOM, RELAX, 5.000000E-01

> OBJ1, NAME, INLET
> OBJ1, POSITION, 0.000000E+00, 0.000000E+00, 0.000000E+00
> OBJ1, SIZE, 0.000000E+00, 3.300000E-01, 7.600000E-01
> OBJ1, CLIPART, cube3t
> OBJ1, ROTATION24, 1
> OBJ1, TYPE, USER_DEFINED

> OBJ2, NAME, OUTLET
> OBJ2, POSITION, 3.800000E+00, 0.000000E+00, 0.000000E+00
> OBJ2, SIZE, 0.000000E+00, 3.300000E-01, 7.600000E-01
> OBJ2, CLIPART, cube12t
> OBJ2, ROTATION24, 1
> OBJ2, TYPE, USER_DEFINED

```

> OBJ3, NAME, VWAL1
> OBJ3, POSITION, 0.000000E+00, 0.000000E+00, 0.000000E+00
> OBJ3, SIZE, 3.800000E+00, 0.000000E+00, 7.600000E-01
> OBJ3, CLIPART, cube11
> OBJ3, ROTATION24, 1
> OBJ3, TYPE, PLATE
> OBJ3, ADIABATIC, 0.000000E+00, 0.000000E+00

> OBJ4, NAME, BWAL
> OBJ4, POSITION, 0.000000E+00, 0.000000E+00, 0.000000E+00
> OBJ4, SIZE, 3.800000E+00, 3.300000E-01, 0.000000E+00
> OBJ4, CLIPART, cube11
> OBJ4, ROTATION24, 1
> OBJ4, TYPE, PLATE
> OBJ4, ADIABATIC, 0.000000E+00, 0.000000E+00

> OBJ5, NAME, VWAL2
> OBJ5, POSITION, 0.000000E+00, 3.300000E-01, 0.000000E+00
> OBJ5, SIZE, 3.800000E+00, 0.000000E+00, 7.600000E-01
> OBJ5, CLIPART, cube11
> OBJ5, ROTATION24, 1
> OBJ5, TYPE, PLATE
> OBJ5, ADIABATIC, 0.000000E+00, 0.000000E+00

> OBJ6, NAME, LMP1
> OBJ6, POSITION, 1.987500E+00, 2.125000E-02, 0.000000E+00
> OBJ6, SIZE, 2.500000E-02, 2.500000E-02, 7.600000E-01
> OBJ6, CLIPART, cylinder
> OBJ6, ROTATION24, 1
> OBJ6, TYPE, BLOCKAGE
> OBJ6, MATERIAL, 198

> OBJ7, NAME, LMP2
> OBJ7, POSITION, 1.987500E+00, 9.625000E-02, 0.000000E+00
> OBJ7, SIZE, 2.500000E-02, 2.500000E-02, 7.600000E-01
> OBJ7, CLIPART, cylinder
> OBJ7, ROTATION24, 1
> OBJ7, TYPE, BLOCKAGE
> OBJ7, MATERIAL, 198

> OBJ8, NAME, LMP3
> OBJ8, POSITION, 1.987500E+00, 1.712500E-01, 0.000000E+00
> OBJ8, SIZE, 2.500000E-02, 2.500000E-02, 7.600000E-01
> OBJ8, CLIPART, cylinder
> OBJ8, ROTATION24, 1
> OBJ8, TYPE, BLOCKAGE
> OBJ8, MATERIAL, 198

> OBJ9, NAME, LMP4
> OBJ9, POSITION, 1.987500E+00, 2.462500E-01, 0.000000E+00
> OBJ9, SIZE, 2.500000E-02, 2.500000E-02, 7.600000E-01
> OBJ9, CLIPART, cylinder
> OBJ9, ROTATION24, 1
> OBJ9, TYPE, BLOCKAGE
> OBJ9, MATERIAL, 198

> OBJ10, NAME, LMP6

> OBJ10, POSITION, 2.112500E+00, 1.310000E-01, 0.000000E+00
> OBJ10, SIZE, 2.500000E-02, 2.500000E-02, 7.600000E-01
> OBJ10, CLIPART, cylinder
> OBJ10, ROTATION24, 1
> OBJ10, TYPE, BLOCKAGE
> OBJ10, MATERIAL, 198

> OBJ11, NAME, LMP7
> OBJ11, POSITION, 2.112500E+00, 5.850000E-02, 0.000000E+00
> OBJ11, SIZE, 2.500000E-02, 2.500000E-02, 7.600000E-01
> OBJ11, CLIPART, cylinder
> OBJ11, ROTATION24, 1
> OBJ11, TYPE, BLOCKAGE
> OBJ11, MATERIAL, 198

> OBJ12, NAME, LMP8
> OBJ12, POSITION, 2.112500E+00, 2.085000E-01, 0.000000E+00
> OBJ12, SIZE, 2.500000E-02, 2.500000E-02, 7.600000E-01
> OBJ12, CLIPART, cylinder
> OBJ12, ROTATION24, 1
> OBJ12, TYPE, BLOCKAGE
> OBJ12, MATERIAL, 198

> OBJ13, NAME, LMP9
> OBJ13, POSITION, 2.112500E+00, 2.835000E-01, 0.000000E+00
> OBJ13, SIZE, 2.500000E-02, 2.500000E-02, 7.600000E-01
> OBJ13, CLIPART, cylinder
> OBJ13, ROTATION24, 1
> OBJ13, TYPE, BLOCKAGE
> OBJ13, MATERIAL, 198

> OBJ14, NAME, LP11
> OBJ14, POSITION, 2.237500E+00, 2.125000E-02, 0.000000E+00
> OBJ14, SIZE, 2.500000E-02, 2.500000E-02, 7.600000E-01
> OBJ14, CLIPART, cylinder
> OBJ14, ROTATION24, 1
> OBJ14, TYPE, BLOCKAGE
> OBJ14, MATERIAL, 198

> OBJ15, NAME, LP12
> OBJ15, POSITION, 2.237500E+00, 9.625000E-02, 0.000000E+00
> OBJ15, SIZE, 2.500000E-02, 2.500000E-02, 7.600000E-01
> OBJ15, CLIPART, cylinder
> OBJ15, ROTATION24, 1
> OBJ15, TYPE, BLOCKAGE
> OBJ15, MATERIAL, 198

> OBJ16, NAME, LP13
> OBJ16, POSITION, 2.237500E+00, 1.712500E-01, 0.000000E+00
> OBJ16, SIZE, 2.500000E-02, 2.500000E-02, 7.600000E-01
> OBJ16, CLIPART, cylinder
> OBJ16, ROTATION24, 1
> OBJ16, TYPE, BLOCKAGE
> OBJ16, MATERIAL, 198

> OBJ17, NAME, LP14
> OBJ17, POSITION, 2.237500E+00, 2.462500E-01, 0.000000E+00
> OBJ17, SIZE, 2.500000E-02, 2.500000E-02, 7.600000E-01

> OBJ17, CLIPART, cylinder
> OBJ17, ROTATION24, 1
> OBJ17, TYPE, BLOCKAGE
> OBJ17, MATERIAL, 198

> OBJ18, NAME, LP16
> OBJ18, POSITION, 2.362500E+00, 1.310000E-01, 0.000000E+00
> OBJ18, SIZE, 2.500000E-02, 2.500000E-02, 7.600000E-01
> OBJ18, CLIPART, cylinder
> OBJ18, ROTATION24, 1
> OBJ18, TYPE, BLOCKAGE
> OBJ18, MATERIAL, 198

> OBJ19, NAME, LP17
> OBJ19, POSITION, 2.362500E+00, 5.850000E-02, 0.000000E+00
> OBJ19, SIZE, 2.500000E-02, 2.500000E-02, 7.600000E-01
> OBJ19, CLIPART, cylinder
> OBJ19, ROTATION24, 1
> OBJ19, TYPE, BLOCKAGE
> OBJ19, MATERIAL, 198

> OBJ20, NAME, LP18
> OBJ20, POSITION, 2.362500E+00, 2.085000E-01, 0.000000E+00
> OBJ20, SIZE, 2.500000E-02, 2.500000E-02, 7.600000E-01
> OBJ20, CLIPART, cylinder
> OBJ20, ROTATION24, 1
> OBJ20, TYPE, BLOCKAGE
> OBJ20, MATERIAL, 198

> OBJ21, NAME, LP19
> OBJ21, POSITION, 2.362500E+00, 2.835000E-01, 0.000000E+00
> OBJ21, SIZE, 2.500000E-02, 2.500000E-02, 7.600000E-01
> OBJ21, CLIPART, cylinder
> OBJ21, ROTATION24, 1
> OBJ21, TYPE, BLOCKAGE
> OBJ21, MATERIAL, 198

> OBJ22, NAME, LP21
> OBJ22, POSITION, 2.487500E+00, 2.125000E-02, 0.000000E+00
> OBJ22, SIZE, 2.500000E-02, 2.500000E-02, 7.600000E-01
> OBJ22, CLIPART, cylinder
> OBJ22, ROTATION24, 1
> OBJ22, TYPE, BLOCKAGE
> OBJ22, MATERIAL, 198

> OBJ23, NAME, LP22
> OBJ23, POSITION, 2.487500E+00, 9.625000E-02, 0.000000E+00
> OBJ23, SIZE, 2.500000E-02, 2.500000E-02, 7.600000E-01
> OBJ23, CLIPART, cylinder
> OBJ23, ROTATION24, 1
> OBJ23, TYPE, BLOCKAGE
> OBJ23, MATERIAL, 198

> OBJ24, NAME, LP23
> OBJ24, POSITION, 2.487500E+00, 1.712500E-01, 0.000000E+00
> OBJ24, SIZE, 2.500000E-02, 2.500000E-02, 7.600000E-01
> OBJ24, CLIPART, cylinder
> OBJ24, ROTATION24, 1

> OBJ24, TYPE, BLOCKAGE
> OBJ24, MATERIAL, 198

> OBJ25, NAME, LP24
> OBJ25, POSITION, 2.487500E+00, 2.462500E-01, 0.000000E+00
> OBJ25, SIZE, 2.500000E-02, 2.500000E-02, 7.600000E-01
> OBJ25, CLIPART, cylinder
> OBJ25, ROTATION24, 1
> OBJ25, TYPE, BLOCKAGE
> OBJ25, MATERIAL, 198

> OBJ26, NAME, BAFL1
> OBJ26, POSITION, 2.118750E+00, 0.000000E+00, 0.000000E+00
> OBJ26, SIZE, 1.250000E-02, 3.375000E-02, 7.600000E-01
> OBJ26, CLIPART, cube14
> OBJ26, ROTATION24, 1
> OBJ26, TYPE, BLOCKAGE
> OBJ26, MATERIAL, 198

> OBJ27, NAME, BAFL2
> OBJ27, POSITION, 2.368750E+00, 0.000000E+00, 0.000000E+00
> OBJ27, SIZE, 1.250000E-02, 3.375000E-02, 7.600000E-01
> OBJ27, CLIPART, cube14
> OBJ27, ROTATION24, 1
> OBJ27, TYPE, BLOCKAGE

> OBJ28, NAME, BAFR1
> OBJ28, POSITION, 1.993750E+00, 2.962500E-01, 0.000000E+00
> OBJ28, SIZE, 1.250000E-02, 3.375000E-02, 7.600000E-01
> OBJ28, CLIPART, cube14
> OBJ28, ROTATION24, 1
> OBJ28, TYPE, BLOCKAGE
> OBJ28, MATERIAL, 198

> OBJ29, NAME, BAFR2
> OBJ29, POSITION, 2.243750E+00, 2.962500E-01, 0.000000E+00
> OBJ29, SIZE, 1.250000E-02, 3.375000E-02, 7.600000E-01
> OBJ29, CLIPART, cube14
> OBJ29, ROTATION24, 1
> OBJ29, TYPE, BLOCKAGE
> OBJ29, MATERIAL, 198

> OBJ30, NAME, BAFR3
> OBJ30, POSITION, 2.493750E+00, 2.962500E-01, 0.000000E+00
> OBJ30, SIZE, 1.250000E-02, 3.375000E-02, 7.600000E-01
> OBJ30, CLIPART, cube14
> OBJ30, ROTATION24, 1
> OBJ30, TYPE, BLOCKAGE
> OBJ30, MATERIAL, 198

M
STOP